

Electron-impact ionization of W^{9+} and W^{10+}

Runjia Bao(鲍润家), Junkui Wei(魏军奎), Lei Chen(陈雷), Bowen Li(李博文), and Ximeng Chen(陈熙萌)
Citation: Chin. Phys. B, 2023, 32 (**6**): 063401. DOI: 10.1088/1674-1056/aca14d
Journal homepage: http://cpb.iphy.ac.cn; http://iopscience.iop.org/cpb

What follows is a list of articles you may be interested in

Debye-screening effect on electron-impact excitation of helium-like Al^{11+} and Fe^{24+} ions

Yu-Long Ma(马玉龙), Ling Liu(刘玲), Lu-You Xie(颉录有), Yong Wu(吴勇), Deng-Hong Zhang(张登红), Chen-Zhong Dong(董晨钟), Yi-Zhi Qu(屈一至), and Jian-Guo Wang(王建国)
Chin. Phys. B, 2022, 31 (**4**): 043401. DOI: 10.1088/1674-1056/ac2e65

Electron-impact ionization cross section calculations for lithium-like ions

Guo-Jie Bian(卞国杰), Jyh-Ching Chang(张稚卿), Ke-Ning Huang(黄克宁), Chen-Sheng Wu(武晨晟), Yong-Jun Cheng(程勇军), Kai Wang(王凯), and Yong Wu(吴勇)
Chin. Phys. B, 2022, 31 (**1**): 013401. DOI: 10.1088/1674-1056/ac229e

Electron-impact single ionizaiton for W^{4+} and W^{5+}

Denghong Zhang(张登红), Luyou Xie(颉录有), Jun Jiang(蒋军), Zhongwen Wu(武中文), Chenzhong Dong(董晨钟), Yinglong Shi(师应龙), Yizhi Qu(屈一至)
Chin. Phys. B, 2018, 27 (**5**): 053402. DOI: 10.1088/1674-1056/27/5/053402

Fast-electron-impact ionization process by 3p of hydrogen-like ions in Debye plasmas

Qi Yue-Ying (祁月盈), Ye Dan-Dan (叶丹丹), Wang Jian-Guo (王建国), Qu Yi-Zhi (屈一至)
Chin. Phys. B, 2015, 24 (**3**): 033403. DOI: 10.1088/1674-1056/24/3/033403

Ionization cross sections for electron scattering from metastable rare-gas atoms (Ne^* and Ar^*)

Zhang Yong-Zhi (张永志), Zhou Ya-Jun (周雅君)
Chin. Phys. B, 2013, 22 (**7**): 073402. DOI: 10.1088/1674-1056/22/7/073402

Electron-impact ionization of W^{9+} and W^{10+}

Runjia Bao(鲍润家), Junkui Wei(魏军奎), Lei Chen(陈雷),
Bowen Li(李博文)†, and Ximeng Chen(陈熙萌)

School of Nuclear Science and Technology, Lanzhou University, Lanzhou 730000, *China*

(Received 10 May 2022; revised manuscript received 3 November 2022; accepted manuscript online 9 November 2022)

Electron-impact single-ionization (EISI) cross sections for W^{q+} ($q = 9$, 10) ions have been calculated by using the level-to-level distorted-wave (LLDW) method with emphasis on the contribution of metastable states to the total ionization cross sections. Contributions from direct-ionization (DI) and excitation-autoionization (EA) processes are taken into account. The calculated cross sections include the contributions from both the ground configuration and the long-lived metastable states with lifetimes exceeding 10^{-6} s. Calculated cross sections are in good agreement with experimental measurements when the influence of metastable states on the total ionization cross section are well considered.

Keywords: tungsten ions, electron-impact ionization, relativistic distorted-wave method, metastable states

PACS: 34.50.Fa, 34.80.Dp, 32.80.Aa **DOI:** 10.1088/1674-1056/aca14d

1. Introduction

Because of its low sputtering rate, low tritium absorption and high temperature characteristics,[1–3] tungsten has been used in divertors for magnetic confinement fusion devices such as EAST, HL-2M, LHD, ITER and CFETR. Since the divertor is a plasma-facing component, tungsten will be sputtered into the plasma and become an impurity. To understand its behavior, various reliable atomic data are required for detailed collisional-radiative (CR) modeling.[4–7]

EISI is an important process in determining the ionization balance of non-LTE plasmas. In past years, considerable effort has been made to obtain reliable EISI cross sections both experimentally and theoretically (see review paper[6] and reference therein). Due to its importance, International Atomic Energy Agency (IAEA) hosted two meetings on recommended data for tungsten ions in 2021. As concluded in the first meeting, for EISI, "in the experiments ⋯ the effect of long-lived excited states (in the parent ion beam) will be presented in the cross-section measurements. ⋯ Theoretical modelling of the resulting cross sections can provide information on the long-lived beam components. Fusion plasma will contain such species in long-lived excited states whose cross sections are needed" (https://amdis.iaea.org/meetings/tm-tungsten-hydrogen/). The influence of the metastable states exists in the low charged states of tungsten. Hence metastable levels could have a considerable influence on the divertor plasma where the dominant charged states are W^{1+}–W^{15+}.[8,9]

In the 2018, Zhang *et al.* calculated the EISI cross sections for W^{4+} and W^{5+} using detailed LLDW method.[10] However, their calculated total cross sections are much larger than the experiment data. Theoretical and experimental studies on the W^{5+} were subsequently reported by Jonauskas *et al.*, and they found that the metastable states $5p^5 5d^2$ and $4f^{13} 5d^2$ contributed greatly to the total cross section.[11] Detailed LLDW calculations for W^{7+} were reported by Chen *et al.* with emphasis on the contribution of metastable states to the total EISI cross section.[12] Moreover, in a recent experiment, Yan *et al.* observed the W^{7+} line at 574.47 nm at 48 eV in the electron-beam ion trap (EBIT) plasma, which is far below the W^{5+} (65 eV) and W^{6+} (122 eV) ionization thresholds, confirmed the significantly contribution of the metastable levels to the low energies tungsten plasmas.[13]

As for W^{9+} and W^{10+}, recently, Priti *et al.* measured and analyzed the visible lines for W^{8+} and W^{9+} ions,[14] and Lu *et al.* presented the visible lines from W^{10+}.[15] But contribution from the metastable states to the total cross sections for W^{9+} and W^{10+} remain unclear. It should be noted that due to open 4f subshell involved, theoretical calculation is challenging and no level energies available for comparison in W^{9+} and W^{10+} in the NIST ASD.[16]

Therefore, the main aim of our work is to determine the contribution of the metastable states on the total EISI cross sections for W^{9+} and W^{10+}. The atomic energy levels and radiative transition probabilities were calculated by using the fully relativistic flexible atomic code (FAC), while the autoionization rates and election-impact excitations rates were calculated within the distorted-wave approximation by using FAC.[17] The calculated atomic data were adopted to calculate the level-to-level EISI cross section by using a homemade program as massive data were involved.

†Corresponding author. E-mail: libw@lzu.edu.cn

© 2023 Chinese Physical Society and IOP Publishing Ltd

2. Theoretical methods

DI and EA processes are included to obtain the EISI cross sections from level i of the W^{q+} ion to level j of W^{q+1}

$$\sigma_{ij}(\varepsilon) = \sigma_{ij}^{\mathrm{DI}}(\varepsilon) + \sum_k \sigma_{ik}^{\mathrm{EIE}}(\varepsilon) B_{kj}^{\mathrm{a}}, \tag{1}$$

where ε is the energy of the incident electron, $\sigma_{ij}^{\mathrm{DI}}(\varepsilon)$ is the DI cross section, $\sigma_{ik}^{\mathrm{EIE}}$ is the electron-impact excitation (EIE) cross section to the intermediate level k of the initial ion, and B_{kj}^{a} is the autoionization branching ratio from level k to the final level j, which can be expressed as

$$B_{kj}^{\mathrm{a}} = \frac{A_{kj}^{\mathrm{a}}}{\sum_m A_{km}^{\mathrm{r}} + \sum_n A_{kn}^{\mathrm{a}}}, \tag{2}$$

while A_{kj}^{a} is the autoionization (AI) rate from k of W^{q+} to any level j of W^{q+1}, A_{km}^{r} is the radiative transition (RT) rate of W^{q+} from k to m, and A_{kn}^{a} is the AI rate from k of W^{q+} to any level n of W^{q+1}.

DI cross section at the incident electron energy ε is determined by the follow equation:[17]

$$\sigma_{ij}^{\mathrm{DI}}(\varepsilon) = \frac{1}{k_i^2 g_i} \Omega_{ij}, \tag{3}$$

where k_i and g_i are the kinetic momentum of the incident electron and the statistical weight of the initial state, respectively. Ω_{ij} is the collision strength.

EA cross section $\sigma_{ik}^{\mathrm{EIE}}(\varepsilon)$ at the incident electron energy ε can be expressed as[17]

$$\sigma_{ik}^{\mathrm{EIE}}(\varepsilon) = \frac{\pi}{k_i^2 g_i} \Omega_{ik}, \tag{4}$$

where Ω_{ik} is the collision strength.

3. Results and discussion

Regarding the experiment data, all levels are relevant that have lifetimes larger than the flight time of the ions (usually of the order of a few microseconds) through the setup. Hence we included the levels with lifetime lager than 10^{-6} s into consideration (long-lived levels).

3.1. W^{9+}

There are 5 levels from [Cd] $4f^{14}5s^25p^3$ configuration, 30 levels from the excited [Cd] $4f^{13}5s^25p^4$ configuration and 40 levels from excited [Cd] $4f^{14}5s^25p^25d$ configuration (Table 1 presents the long-lived levels of W^{9+}). Figure 1 shows the level energies of the lowest energy configurations and double ionization threshold of the W^{9+} ion.

For W^{9+}, as mentioned by Stenke *et al.*,[18] the observed threshold energy of 150–160 eV. The ionization potential of the [Cd] $4f^{14}5s^25p^3$ ground state is 176.57 eV, while the calculated single ionization thresholds of the metastable configuration [Cd] $4f^{14}5s^25p^25d$ and [Cd] $4f^{13}5p^4$ are 131.15 eV and 174.13 eV, respectively. To reproduce the experimental ionization cross section and test the reliability of the theoretical approaches, it is necessary to consider not only the ground state of the W^{9+} ion but also all possible (long-lived) excited levels of W^{9+} ions.

Table 1. Long-lived levels of W^{9+} and associated lifetimes. Only levels with lifetime over 10^{-6} s are presented. Note that $a \pm b \equiv a \times 10^{\pm b}$.

Configuration	Index	Level	J	Energy (eV)	Lifetime (s)
$4f^{14}5s^25p^3$	0	$5p_+$	3/2	0.000	∞
	1	$(5p_-)_{1/2}5p_+^2$	3/2	10.133	3.648–4
	2	$(5p_-)_{1/2}5p_+^2$	5/2	12.293	7.596–5
	3	$(5p_-)_{1/2}5p_+^2$	1/2	15.015	2.752-5
	4	$5p_+^3$	3/2	25.464	8.561–5
$4f^{13}5s^25p^4$	5	$(4f_+^7)_{7/2}5p_+^2$	11/2	2.427	∞
	6	$(4f_+^7)_{7/2}5p_+^2$	9/2	2.584	1.493+2
	7	$(4f_+^7)_{7/2}5p_+^2$	3/2	2.832	2.493+1
	8	$(4f_+^7)_{7/2}5p_+^2$	7/2	3.062	2.172+0
	9	$(4f_+^7)_{7/2}5p_+^2$	5/2	3.617	6.297–1
	10	$(4f_-^5)_{5/2}5p_+^2$	5/2	4.820	1.601–2
	11	$(4f_-^5)_{5/2}5p_+^2$	3/2	5.070	2.132–2
	12	$(4f_-^5)_{5/2}5p_+^2$	1/2	5.090	1.307–2
	13	$(4f_-^5)_{5/2}5p_+^2$	9/2	5.480	4.031–3
	14	$(4f_-^5)_{5/2}5p_+^2$	7/2	5.791	7.009–3
	15	$(4f_+^7)_{7/2}5p_+^2$	7/2	6.783	6.256–3
	16	$(4f_-^5)_{5/2}5p_+^2$	5/2	9.260	3.137–3
	17	$(4f_+^7 5p_-)_3 5p_+^3$	7/2	14.566	5.708-5
	18	$(4f_+^7 5p_-)_3 5p_+^3$	9/2	14.885	5.742–5
	19	$(4f_+^7 5p_-)_3 5p_+^3$	5/2	15.523	6.384-5
	20	$(4f_+^7 5p_-)_4 5p_+^3$	7/2	16.150	8.912–5
	21	$(4f_+^7 5p_-)_4 5p_+^3$	9/2	16.425	9.452-5
	22	$(4f_-^5 5p_-)_3 5p_+^3$	5/2	16.452	5.736–5
	23	$(4f_-^5 5p_-)_3 5p_+^3$	7/2	17.081	7.440-5
	24	$(4f_+^7 5p_-)_4 5p_+^3$	11/2	17.262	8.212–5
	25	$(4f_-^5 5p_-)_3 5p_+^3$	3/2	17.398	5.856-5
	26	$(4f_+^7 5p_-)_4 5p_+^3$	5/2	17.723	7.471–5
	27	$(4f_+^7 5p_-)_3 5p_+^3$	3/2	18.749	7.837-5
	28	$(4f_-^5 5p_-)_2 5p_+^3$	5/2	18.965	8.625–5
	29	$(4f_-^5 5p_-)_2 5p_+^3$	7/2	19.200	6.610–5
	30	$(4f_-^5 5p_-)_3 5p_+^3$	9/2	19.531	8.854–5
	31	$(4f_-^5 5p_-)_2 5p_+^3$	3/2	20.174	7.820–5
	32	$(4f_-^5 5p_-)_2 5p_+^3$	1/2	21.119	7.194–5
	33	$4f_+^7$	7/2	30.936	1.686-5
	34	$4f_-^5$	5/2	32.736	1.688–5
$4f^{14}5s^25p^25d$	1994	$(5p_-5p_+)_2 5d_+$	9/2	58.835	3.380-3
	2004	$(5p_+^2)_2 5d_+$	9/2	70.667	5.857–5

3.1.1. The ground state [Cd] $4f^{14}5p^3$

According to Fig. 1, the DI of W^{9+} includes three subshells of 4f, 5s, and 5p. The LLDW results of DI cross section are presented in Fig. 2. The 4f subshell contributes the most to the total DI cross section. The detailed DI process of W^{9+} ground state can be expressed as

$$e^- + [\mathrm{Pd}]\,5s^25p^34f^{14} \rightarrow [\mathrm{Pd}] \left\{ \begin{array}{c} 5s^25p^34f^{13} \\ 5s^25p^24f^{14} \\ 5s5p^34f^{14} \end{array} \right\} + 2e^-. \tag{5}$$

Based on Fig. 1, the EA contribution in the EISI of W^{9+} involves 5s, 5p, and 4f subshells. For the single ionization, the incident electron energies must exceed 176.6 eV, while the double ionization may occur at energies above 381.8 eV. The LLDW calculated of EA cross sections are presented in Fig. 3.

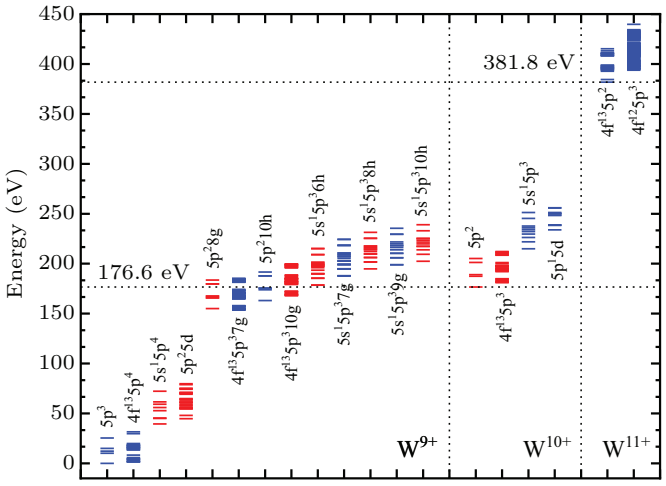


Fig. 1. Energy levels of the main configurations for W^{9+}, W^{10+} and W^{11+}. Red for even configurations, blue for odd configurations. Horizontal dotted lines show single and double ionization thresholds for W^{9+}.

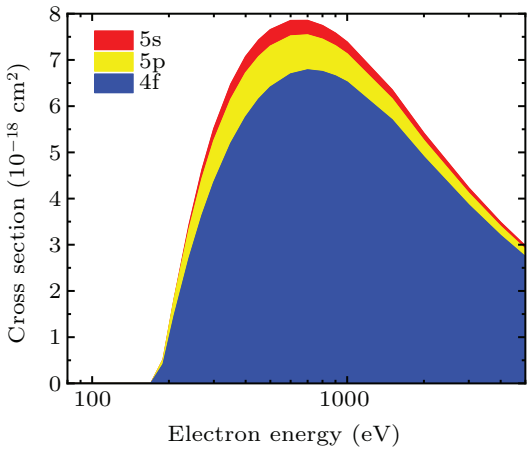


Fig. 2. The contributions of DI cross section from different subshells from W^{9+} ground state. The shadow areas show contributions from different subshells.

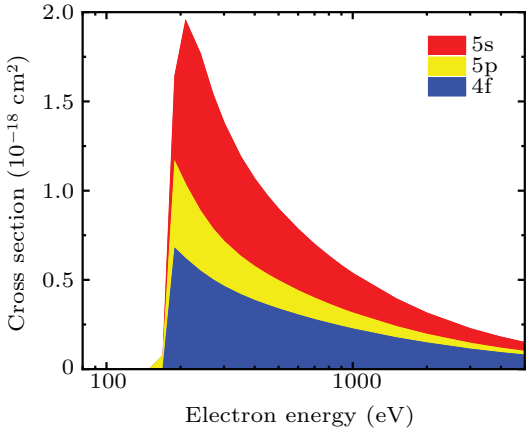


Fig. 3. The contributions of EA cross section from different subshells from W^{9+} ground state. The shadow areas show contributions from different subshells.

For 5s subshell, we considered from 5s→5p at 72.2 eV to 5s→17h at 247.9 eV. Only 71 excited states have energies higher than the first ionization potential 176.6 eV, and the first EA channel is 5s →5g at 198.5 eV. For 5p subshell, we considered from 5p→5d at 79.8 eV to 5p→17h at 200.6 eV. Only 58 excited states have energies higher than the first ionization potential, and the first EA channel is 5p→7g at 177.0 eV.

For 4f subshell, we considered from 4f→5p at 31.5 eV to 4f→17h at 208.8 eV. Only 61 excited states have energies higher than the first ionization potential, and the first EA channel is 4f→7f at 178.8 eV. To check the EA convergence, we calculated the cross sections from the ground state to different nl' and plotted the ratio of nl' in the total EA cross section at the peak of cross section (i.e., 210 eV). We can find in Fig. 4, the proportion of $n = 17$ in total EA cross section is lower than 5%. As n increases, the contribution of the nl' becomes smaller, so we omitted the contribution of the higher nl' in this work. Moreover, we found that when n is larger than 14, the cross sections for W^{9+} obey the following formula:

$$\sigma_{n+1} = \frac{n^3}{(n+1)^3}\sigma_n, \tag{6}$$

where σ_n is the cross section for the shell n. In this way, one can obtain the cross section for higher shells using the extrapolation method.

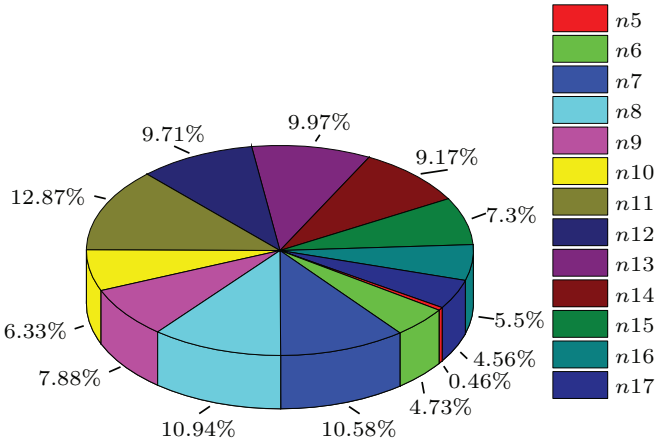


Fig. 4. The ratios of nl' ($n = 5$–17) in the total EA cross section for the W^{9+} ground state [Cd] $4f^{14}5p^3$ at the peak of cross section.

The detailed EA process of W^{9+} ground state can be expressed as

$$e^- + [\mathrm{Pd}]\,5s^2 5p^3 4f^{14} \rightarrow [\mathrm{Pd}] \left\{ \begin{array}{c} 5s^2 5p^3 4f^{13} nl' \\ 5s^2 5p^2 4f^{14} nl' \\ 5s 5p^3 4f^{14} nl' \end{array} \right\} + e^-, \tag{7}$$

where $n \leq 17$ and $l' \leq 5$ (influence of higher nl' has been checked in Fig. 4). AI or TR processes occur in these exci-

tation channels

$$\mathrm{AI} \rightarrow [\mathrm{Pd}] \left\{ \begin{array}{c} 5s^2 5p^2 4f^{14} \\ 5s^2 5p^3 4f^{13} \\ 5s5p^3 4f^{14} \\ 5s^2 5p^2 4f^{13} 5\,[\mathrm{d,f,g}]^1 \\ 5s^2 5p4f^{14} 5\,[\mathrm{d,f,g}]^1 \\ 5s5p^2 4f^{14} 5\,[\mathrm{d,f,g}]^1 \\ 5s^2 5p^2 4f^{13} nl' \\ 5s^2 5p4f^{14} nl' \\ 5s5p^2 4f^{14} nl' \end{array} \right\} + \mathrm{e}^-, \quad (8)$$

$$\mathrm{RT} \rightarrow [\mathrm{Pd}] \left\{ \begin{array}{c} 5s^2 5p^3 4f^{14} \\ 5s^2 5p^4 4f^{13} \\ 5s5p^4 4f^{14} \\ 5s^2 5p^3 4f^{13} 5\,[\mathrm{d,f,g}]^1 \\ 5s^2 5p^2 4f^{14} 5\,[\mathrm{d,f,g}]^1 \\ 5s5p^3 4f^{14} 5\,[\mathrm{d,f,g}]^1 \\ 5s^2 5p^3 4f^{13} nl' \\ 5s^2 5p^2 4f^{14} nl' \\ 5s5p^3 4f^{14} nl' \end{array} \right\} + h\nu. \quad (9)$$

Cross sections are presented in Fig. 5 for the levels associated with the W^{9+} ground state [Cd] $4f^{14}5p^3$ configurations, as listed in Table 1.

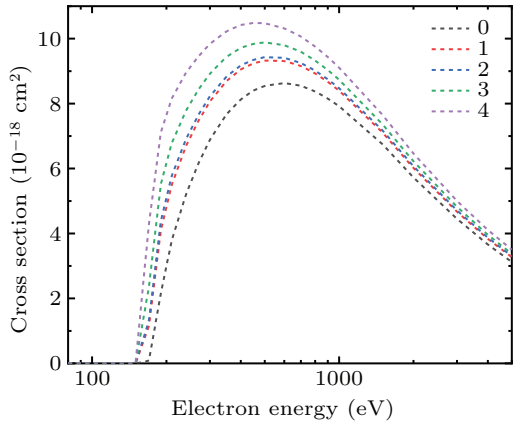


Fig. 5. Cross sections of the long-lived levels of W^{9+} ground state [Cd] $4f^{14}5p^3$ listed in Table 1.

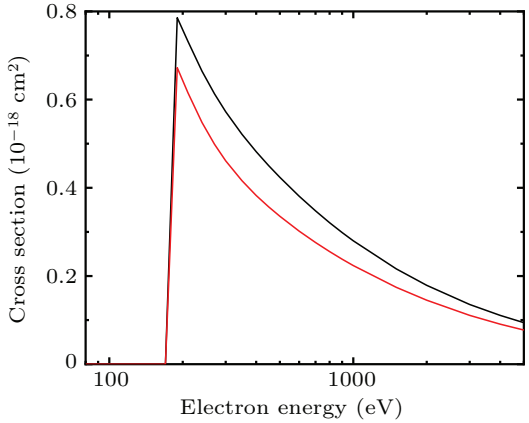


Fig. 6. Effect of electron correlation on the EISI cross section of 4f–*nl* complex for W^{9+} ion. The black solid line: the result of configuration-interaction method includes important singly electron excitation configurations. The red solid line: the result of considering restricted electron correlation within same *n* shell.

Moreover, electron correlation has a big influence on the atomic data hence on the EISI cross sections. But considering the 4f subshell is involved in the calculation, single configuration approximation was adopted in many cases. In the present calculation, restricted electron correlation has been included, i.e., the electron interaction within same *n* shell of the considered complex. We explored the single electron excitation configuration effect in Fig. 6. For example, during calculation of $4f^{13}5s^25p^3n1$ ($n = 7$–17), we set all $4f^{13}5s^25p^35[\mathrm{p,d,f,g}]^1$ and $4f^{13}5s^25p^3n[\mathrm{s,p,d,f,g,h}]^1$ ($n < 18$) as the correlation configuration. The biggest discrepancy is around 14% at the peak position (190 eV), and the difference decreased as energies increased. It should be pointed out, on the one hand, the omitted higher-order correlation, especially the double electron excitation, would have additional effect on the calculated cross sections. On the other hand, electron-correlation will increase the total cross section for some complex while it results in decrease of the total cross section for another complex. Considering that the uncertainties of experimental measurements are general around 30%, current calculations can be trusted.

3.1.2. The metastable state [Cd] $4f^{14}5p^25d$

According to Table 1, there are two levels from [Cd] $4f^{14}5p^25d$ with lifetimes greater than 10^{-6} s. Figure 7 shows the cross section of these two metastable states. DI process of [Cd] $4f^{14}5p^25d$ can be expressed as

$$\mathrm{e}^- + [\mathrm{Pd}]\, 5s^2 5p^2 4f^{14} 5d \rightarrow [\mathrm{Pd}] \left\{ \begin{array}{c} 5s^2 5p^2 4f^{14} \\ 5s^2 5p^2 4f^{13} 5d \\ 5s^2 5p4f^{14} 5d \\ 5s5p^2 4f^{14} 5d \end{array} \right\} + 2\mathrm{e}^-. \quad (10)$$

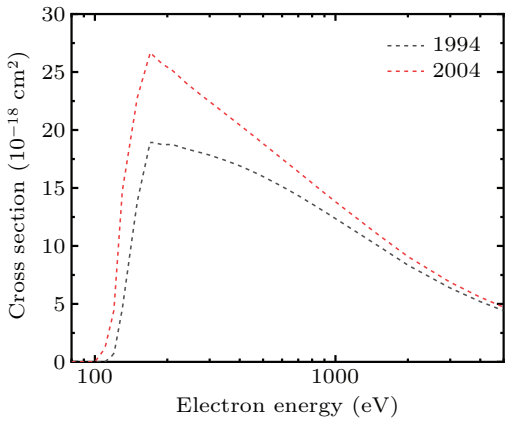


Fig. 7. Cross sections of the long-lived levels of W^{9+} metastable state [Cd]$4f^{14}5p^25d$ listed in Table 1.

The EA contribution in the EISI of [Cd] $4f^{14}5p^25d$ involves 5s, 5p, 4f and 5d subshells. EA process of [Cd] $4f^{14}5p^25d$ can be expressed as

$$\mathrm{e}^- + [\mathrm{Pd}]\, 5s^2 5p^2 4f^{14} 5d \rightarrow [\mathrm{Pd}] \left\{ \begin{array}{c} 5s^2 5p^2 4f^{14} nl' \\ 5s^2 5p^2 4f^{13} 5dnl' \\ 5s^2 5p4f^{14} 5dnl' \\ 5s5p^2 4f^{14} 5dnl' \end{array} \right\} + \mathrm{e}^-, \quad (11)$$

where $n \leq 10$ and $l' \leq 5$. These excitation channels can undergo AI or RT via

$$\mathrm{AI} \rightarrow [\mathrm{Pd}] \left\{ \begin{array}{c} 5s^2 5p^2 4f^{14} \\ 5s^2 5p^3 4f^{13} \\ 5s5p^3 4f^{14} \\ 5s^2 5p^2 4f^{13} 5\,[\mathrm{d,f,g}]^1 \\ 5s^2 5p4f^{14} 5\,[\mathrm{d,f,g}]^1 \\ 5s5p^2 4f^{14} 5\,[\mathrm{d,f,g}]^1 \\ 5s^2 5p^2 4f^{13} nl' \\ 5s^2 5p4f^{14} nl' \\ 5s5p^2 4f^{14} nl' \end{array} \right\} + \mathrm{e}^-, \quad (12)$$

$$\mathrm{RT} \rightarrow [\mathrm{Pd}] \left\{ \begin{array}{c} 5s^2 5p^3 4f^{14} \\ 5s^2 5p^4 4f^{13} \\ 5s5p^4 4f^{14} \\ 5s^2 5p^3 4f^{13} 5\,[\mathrm{d,f,g}]^1 \\ 5s^2 5p^2 4f^{14} 5\,[\mathrm{d,f,g}]^1 \\ 5s5p^3 4f^{14} 5\,[\mathrm{d,f,g}]^1 \\ 5s^2 5p^2 4f^{13} 5d5\,[\mathrm{d,f,g}]^1 \\ 5s^2 5p4f^{14} 5d5\,[\mathrm{d,f,g}]^1 \\ 5s5p^2 4f^{14} 5d5\,[\mathrm{d,f,g}]^1 \\ 5s^2 5p^3 4f^{13} nl' \\ 5s^2 5p^2 4f^{14} nl' \\ 5s5p^3 4f^{14} nl' \\ 5s^2 5p^2 4f^{13} 5dnl' \\ 5s^2 5p4f^{14} 5dnl' \\ 5s5p^2 4f^{14} 5dnl' \end{array} \right\} + h\nu. \quad (13)$$

3.1.3. The metastable state [Cd] $4f^{13}5p^4$

According to Table 1, there are thirty levels from [Cd] $4f^{13}5p^4$ with lifetimes not less than 10^{-6} s. The cross sections of these energy levels are presented in Fig. 8. The DI channel can be expressed as

$$\mathrm{e}^- + [\mathrm{Pd}]\,5s^2 5p^4 4f^{13} \rightarrow [\mathrm{Pd}] \left\{ \begin{array}{c} 5s^2 5p^4 4f^{12} \\ 5s^2 5p^3 4f^{13} \\ 5s5p^4 4f^{13} \end{array} \right\} + 2\mathrm{e}^-. \quad (14)$$

The EA contribution in the EISI of [Cd] $4f^{14}5p5d$ involves 5s, 5p, and 4f subshells. EA process of [Cd] $4f^{13}5p^4$ can be expressed as

$$\mathrm{e}^- + [\mathrm{Pd}]\,5s^2 5p^4 4f^{13} \rightarrow [\mathrm{Pd}] \left\{ \begin{array}{c} 5s^2 5p^4 4f^{12} nl' \\ 5s^2 5p^3 4f^{13} nl' \\ 5s5p^4 4f^{13} nl' \end{array} \right\} + \mathrm{e}^-, \quad (15)$$

where $n \leq 10$ and $l' \leq 5$. These excitation channels can undergo AI or RT via

$$\mathrm{AI} \rightarrow [\mathrm{Pd}] \left\{ \begin{array}{c} 5s^2 5p^2 4f^{14} \\ 5s^2 5p^3 4f^{13} \\ 5s5p^3 4f^{14} \\ 5s^2 5p^2 4f^{13} 5\,[\mathrm{d,f,g}]^1 \\ 5s^2 5p4f^{14} 5\,[\mathrm{d,f,g}]^1 \\ 5s5p^2 4f^{14} 5\,[\mathrm{d,f,g}]^1 \\ 5s^2 5p^2 4f^{13} nl' \\ 5s^2 5p4f^{14} nl' \\ 5s5p^2 4f^{14} nl' \end{array} \right\} + \mathrm{e}^-, \quad (16)$$

$$\mathrm{RT} \rightarrow [\mathrm{Pd}] \left\{ \begin{array}{c} 5s^2 5p^5 4f^{12} \\ 5s^2 5p^4 4f^{13} \\ 5s^2 5p^3 4f^{14} \\ 5s5p^4 4f^{14} \\ 5s5p^5 4f^{13} \\ 5s^2 5p^3 4f^{13} 5\,[\mathrm{d,f,g}]^1 \\ 5s^2 5p^2 4f^{14} 5\,[\mathrm{d,f,g}]^1 \\ 5s5p^3 4f^{14} 5\,[\mathrm{d,f,g}]^1 \\ 5s^2 5p^4 4f^{12} nl' \\ 5s^2 5p^3 4f^{13} nl' \\ 5s5p^4 4f^{13} nl' \end{array} \right\} + h\nu. \quad (17)$$

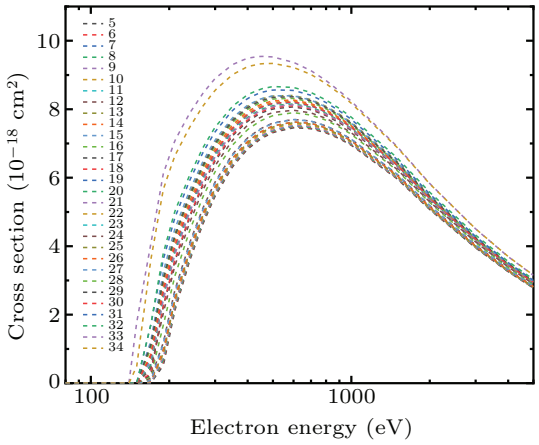


Fig. 8. Cross sections of the long-lived levels of W^{9+} metastable state [Cd]$4f^{13}5p^4$ listed in Table 1.

3.2. W^{10+}

In case of W^{10+}, Stenke *et al.*[18] observed the ionization threshold at 149.9 eV, which is also below their calculated ionization potential of the ground state of 205.8 eV. The present calculated threshold energies are 203.93eV for [Cd] $4f^{14}5p^2$ the ground state and 145.98 eV for the metastable configuration [Cd] $4f^{14}5p5d$ and 199.97 eV for the metastable configuration [Cd] $4f^{13}5p^3$. Like W^{9+}, all possible long-lived excited levels have been considered. The levels are listed in Table 2. Figure 9 shows the energy lowest configurations and the energies of the configuration resulting from the excitation of the ground state and the metastable excitation from the W^{10+} ion.

3.2.1. The ground state [Cd] $4f^{14}5p^2$

According to Fig. 9, the DI of W^{10+} includes three subshells of 4f, 5s, and 5p. The LLDW results of DI cross section are presented in Fig. 10. The 4f subshell contributes the most to the total DI cross section. The detailed DI process of W^{10+} ground state can be expressed as

$$\mathrm{e}^- + [\mathrm{Pd}]\,5s^2 5p^2 4f^{14} \rightarrow [\mathrm{Pd}] \left\{ \begin{array}{c} 5s^2 5p^2 4f^{13} \\ 5s^2 5p4f^{14} \\ 5s5p^2 4f^{14} \end{array} \right\} + 2\mathrm{e}^-. \quad (18)$$

Based on Fig. 9, the EA contribution in the EISI of W^{10+} involves 5s, 5p, and 4f subshells. For single ionization, the excitation energy must exceed 203.9 eV, and the double ion-

ization may occur at energies above 436.1 eV. The LLDW calculation of EA cross section are presented in Fig. 11.

Table 2. Long-lived levels of W^{10+} and associated lifetimes. Only levels with lifetime over 10^{-6} s are presented. Note that $a \pm b \equiv a \times 10^{\pm b}$.

Configuration	Index	Level	J	Energy (eV)	Lifetime (s)
$4f^{14}5s^25p^2$	0	$5p_-^2$	0	0.000	∞
	1	$(5p_-)_{1/2}5p_+$	1	10.790	1.119–4
	2	$(5p_-)_{1/2}5p_+$	2	12.516	3.097–3
	3	$5p_+^2$	2	24.716	4.809–5
	4	$5p_+^2$	0	28.665	2.537–5
$4f^{13}5s^25p^3$	5	$(4f_+^7)_{7/2}5p_+$	5	5.270	∞
	6	$(4f_+^7)_{7/2}5p_+$	2	5.881	4.809–1
	7	$(4f_+^7)_{7/2}5p_+$	3	6.121	1.658+1
	8	$(4f_+^7)_{7/2}5p_+$	4	6.839	1.014–1
	9	$(4f_-^5)_{5/2}5p_+$	1	7.254	2.470–2
	10	$(4f_-^5)_{5/2}5p_+$	4	8.437	3.824–3
	11	$(4f_-^5)_{5/2}5p_+$	2	9.095	4.589-3
	12	$(4f_-^5)_{5/2}5p_+$	3	9.351	5.308–3
	13	$(4f_+^7 5p_-)_3 5p_+^2$	5	16.466	7.253–5
	14	$(4f_+^7 5p_-)_3 5p_+^2$	4	17.117	7.393–5
	15	$(4f_+^7 5p_-)_4 5p_+^2$	2	17.359	6.991–5
	16	$(4f_+^7 5p_-)_4 5p_+^2$	3	17.715	7.086–5
	17	$(4f_-^5 5p_-)_3 5p_+^2$	1	18.665	7.221–5
	18	$(4f_-^5 5p_-)_3 5p_+^2$	2	18.727	7.514–5
	19	$(4f_+^7 5p_-)_4 5p_+^2$	5	19.006	2.648–4
	20	$(4f_+^7 5p_-)_4 5p_+^2$	4	19.075	1.525–4
	21	$(4f_-^5 5p_-)_3 5p_+^2$	3	19.098	9.090–5
	22	$(4f_+^7 5p_-)_4 5p_+^2$	6	19.141	2.706–4
	23	$(4f_+^7 5p_-)_3 5p_+^2$	1	19.356	2.845–4
	24	$(4f_+^7 5p_-)_3 5p_+^2$	3	19.760	1.762–4
	25	$(4f_+^7 5p_-)_3 5p_+^2$	2	19.849	2.202–4
	26	$(4f_-^5 5p_-)_2 5p_+^2$	4	19.866	7.579–5
	27	$(4f_-^5 5p_-)_3 5p_+^2$	5	21.370	3.012–4
	28	$(4f_-^5 5p_-)_2 5p_+^2$	2	21.597	2.060–4
	29	$(4f_-^5 5p_-)_2 5p_+^2$	3	21.625	1.202–4
	30	$(4f_-^5 5p_-)_3 5p_+^2$	4	21.826	1.964-4
	31	$(4f_-^5 5p_-)_2 5p_+^2$	1	22.148	2.262–4
	32	$(4f_-^5 5p_-)_2 5p_+^2$	0	22.324	2.264-4
	33	$(4f_+^7 5p_-)_3 5p_+^2$	3	22.657	6.773–5
	34	$(4f_+^7 5p_-)_4 5p_+^2$	4	22.922	6.895-5
	35	$(4f_-^5 5p_-)_3 5p_+^2$	3	24.694	7.177–5
	36	$(4f_-^5 5p_-)_2 5p_+^2$	2	25.724	5.926–5
	37	$(4f_+^7)_{7/2}5p_+^3$	4	32.971	2.333–5
	38	$(4f_+^7)_{7/2}5p_+^3$	3	33.241	2.318–5
	39	$(4f_+^7)_{7/2}5p_+^3$	5	33.700	2.259–5
	40	$(4f_-^5)_{5/2}5p_+^3$	3	34.592	2.318–5
	41	$(4f_+^7)_{5/2}5p_+^3$	2	35.365	2.209–5
	42	$(4f_-^5)_{5/2}5p_+^3$	2	35.709	2.219–5
	43	$(4f_-^5)_{5/2}5p_+^3$	4	36.385	2.215–5
	44	$(4f_-^5)_{5/2}5p_+^3$	1	36.740	2.236–5
$4f^{14}5s^25p5d$	2528	$(5p_+^1)_{3/2}5d_+^1$	4	72.376	1.246–4

For 5s subshell, we considered from 5s→5p at 74.3 eV to 5s→14h at 263.3 eV. Only 51 excited states have energy higher than the first ionization potential 203.9 eV, and the first EA channel is 5s→5g at 207.2 eV. For 5p subshell, we considered from 5p→5d at 79.3 eV to 5p→14h at 213.2 eV. Only 23 excited states have energy higher than the first ionization potential, and the first EA channel is 5p→10h at 204.9 eV. This is why 5p→ nl' shows few contributions in Fig. 11.

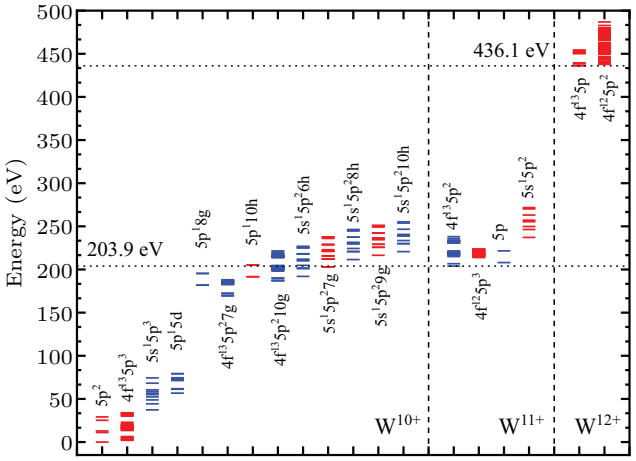


Fig. 9. Energy levels of the main configurations for W^{10+}, W^{11+} and W^{12+}. Red for even configurations, and blue for odd configurations. Horizontal dotted lines show single and double ionization thresholds for W^{10+}.

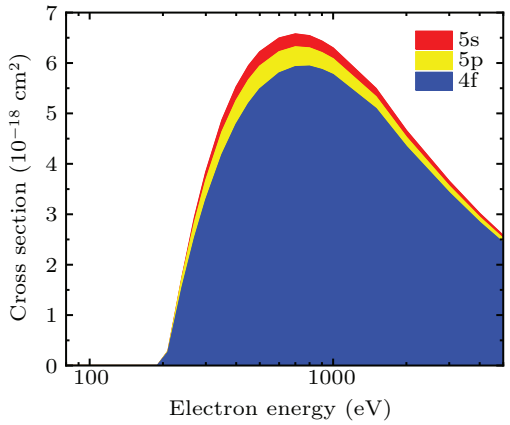


Fig. 10. Accumulated DI cross sections of the ground state W^{10+}. The shadow areas show contributions from different subshells.

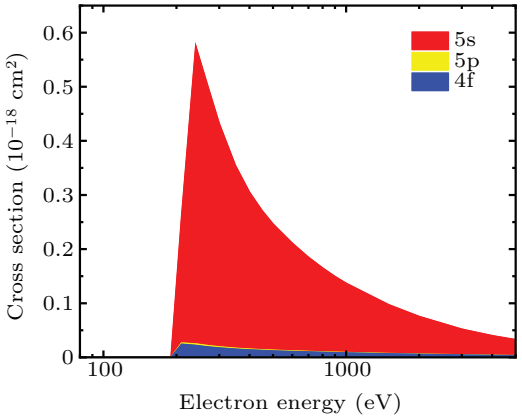


Fig. 11. Accumulated EA cross sections of the ground state W^{10+}. The shadow areas show contributions from different subshells.

For 4f subshell, we considered from 4f→5p at 34.0 eV to 4f→14h at 229.7 eV. Only 39 excited states have energy higher than the first ionization potential 203.9 eV, and the first one is 4f→7h at 204.8 eV. Then we calculated the cross sections from the ground state to different nl' and plotted the ratio

of nl' in the total EA cross section at the peak of cross section (i.e., 240 eV). We can see in Fig. 12 that the proportion of $n = 14$ is smaller than 5%. Hence contributions of $n > 15$ were ignored in this work. In addition, we confirm that the same scaling rule determined by Eq. (6) can be adopted for $n > 12$ for W^{10+}.

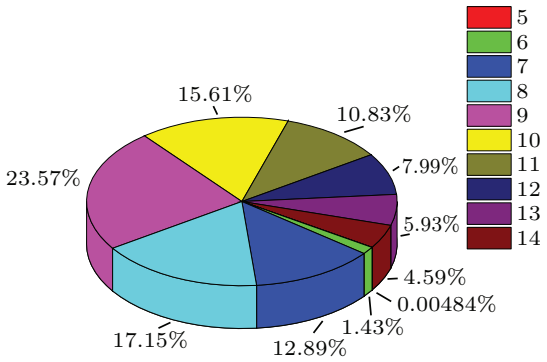


Fig. 12. The ratios of nl' ($n = 5$–14) in the total EA cross section for the W^{10+} ground state [Cd] $4f^{14}5p^2$ at the peak of cross section.

The detailed EA process of W^{10+} ground state can be expressed as

$$e^- + [Pd]\,5s^25p^24f^{14} \rightarrow [Pd]\left\{\begin{array}{c} 5s^25p^24f^{13}nl' \\ 5s^25p4f^{14}nl' \\ 5s5p^24f^{14}nl' \end{array}\right\} + e^-, \quad (19)$$

where $n \leq 14$ and $l' \leq 5$ (influence of higher nl' has been checked in Fig. 12). These excitation channels can be performed via AI or RT

$$\mathrm{AI} \rightarrow [Pd]\left\{\begin{array}{c} 5s^25p^24f^{13} \\ 5s^25p^34f^{12} \\ 5s^25p4f^{14} \\ 5s5p^34f^{13} \\ 5s5p^24f^{14} \\ 5s^25p^24f^{12}5[d,f,g]1 \\ 5s^25p4f^{13}5\,[d,f,g]\,1 \\ 5s5p^24f^{13}5[d,f,g]1 \\ 5s^25p^24f^{12}nl' \\ 5s^25p4f^{13}nl' \\ 5s5p^24f^{13}nl' \end{array}\right\} + e^-, \quad (20)$$

$$\mathrm{RT} \rightarrow [Pd]\left\{\begin{array}{c} 5s^25p^24f^{14} \\ 5s5p^34f^{14} \\ 5s^25p^34f^{13} \\ 5s^25p^24f^{13}5\,[d,f,g]\,1 \\ 5s^25p4f^{14}5\,[d,f,g]\,1 \\ 5s5p^24f^{14}5\,[d,f,g]\,1 \\ 5s^25p^24f^{13}nl' \\ 5s^25p4f^{14}nl' \\ 5s5p^24f^{14}nl' \end{array}\right\} + h\nu. \quad (21)$$

Cross sections are presented in Fig. 13 for the levels associated with the W^{10+} ground state [Cd] $4f^{14}5p^2$ configurations, as listed in Table 2.

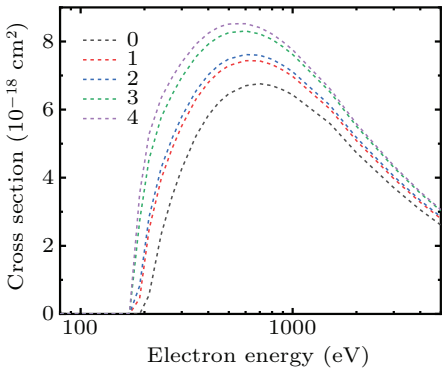


Fig. 13. Cross sections of the long-lived levels of W^{10+} ground state [Cd]$4f^{14}5p^2$ listed in Table 2.

3.2.2. The metastable state [Cd] $4f^{14}5p5d$

According to Table 2, for metastable state [Cd] $4f^{14}5p5d$, there is only one energy level's lifetime greater than 10^{-6} s. Similarly, DI process of [Cd] $4f^{14}5p5d$ can be expressed as

$$e^- + [Pd]\,5s^25p4f^{14}5d \rightarrow [Pd]\left\{\begin{array}{c} 5s^25p4f^{14} \\ 5s^25p4f^{13}5d \\ 5s^24f^{14}5d \\ 5s5p4f^{14}5d \end{array}\right\} + 2e^-. \quad (22)$$

The EA contribution in the EISI of [Cd] $4f^{14}5p5d$ involves 5s, 5p, 4f and 5d subshells. EA process of [Cd] $4f^{14}5p5d$ can be expressed as

$$e^- + [Pd]\,5s^25p4f^{14}5d \rightarrow [Pd]\left\{\begin{array}{c} 5s^25p4f^{14}nl' \\ 5s^25p4f^{13}5dnl' \\ 5s^24f^{14}5dnl' \\ 5s5p4f^{14}5dnl' \end{array}\right\} + e^-, \quad (23)$$

where $n \leq 10$ and $l' \leq 5$. These excitation channels can be performed via AI or RT

$$\mathrm{AI} \rightarrow [Pd]\left\{\begin{array}{c} 5s^25p^24f^{13} \\ 5s^25p^34f^{12} \\ 5s5p^34f^{13} \\ 5s^25p^24f^{12}5[d,f,g]1 \\ 5s^25p4f^{13}5\,[d,f,g]\,1 \\ 5s5p^24f^{13}5[d,f,g]1 \\ 5s^25p^24f^{12}nl' \\ 5s^25p4f^{13}nl' \\ 5s5p^24f^{13}nl' \end{array}\right\} + e^-, \quad (24)$$

$$\mathrm{RT} \rightarrow [Pd]\left\{\begin{array}{c} 5s^25p^24f^{14} \\ 5s^25p^34f^{13} \\ 5s5p^34f^{14} \\ 5s^25p^24f^{13}5[d,f,g]1 \\ 5s^25p4f^{14}5\,[d,f,g]\,1 \\ 5s5p^24f^{14}5\,[d,f,g]\,1 \\ 5s^25p4f^{13}5d5[d,f,g]1 \\ 5s^24f^{14}5d5[d,f,g]1 \\ 5s5p4f^{14}5d5\,[d,f,g]\,1 \\ 5s^25p^24f^{13}nl' \\ 5s^25p4f^{14}nl' \\ 5s5p^24f^{14}nl' \\ 5s^25p4f^{14}nl' \\ 5s^25p4f^{13}5dnl' \\ 5s^24f^{14}5dnl' \\ 5s5p4f^{14}5dnl' \end{array}\right\} + h\nu. \quad (25)$$

3.2.3. The metastable state [Cd] $4f^{13}5p^3$

According to Table 2, there are forty levels from [Cd] $4f^{13}5p^3$ with lifetimes not less than 10^{-6} s. Figure 14 shows the cross section of these forty metastable states. DI process of [Cd] $4f^{13}5p^3$ can be expressed as

$$e^- + [Pd]\,5s^25p^34f^{13} \rightarrow [Pd]\left\{\begin{array}{c}5s^25p^34f^{12}\\5s^25p^24f^{13}\\5s5p^34f^{13}\end{array}\right\} + 2e^-. \quad (26)$$

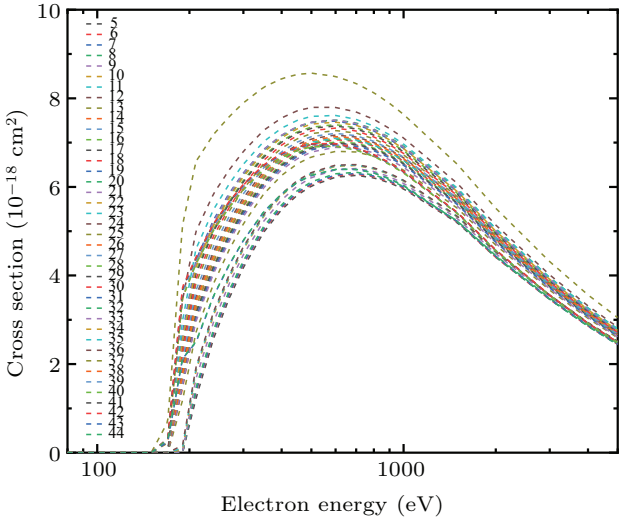


Fig. 14. Cross sections of the long-lived levels of W^{10+} metastable state [Cd]$4f^{13}5p^3$ listed in Table 2.

The EA contribution in the EISI of [Cd] $4f^{13}5p^3$ involves 5s, 5p and 4f subshells. EA process of [Cd] $4f^{13}5p^3$ can be expressed as

$$e^- + [Pd]\,5s^25p^34f^{13} \rightarrow [Pd]\left\{\begin{array}{c}5s^25p^34f^{12}nl'\\5s^25p^24f^{13}nl'\\5s5p^34f^{13}nl'\end{array}\right\} + e^-, \quad (27)$$

where $n \leq 10$ and $l' \leq 5$. These excitation channels can be performed via AI or RT

$$AI \rightarrow [Pd]\left\{\begin{array}{c}5s^25p^24f^{13}\\5s^25p^34f^{12}\\5s5p^34f^{13}\\5s^25p^24f^{12}5[d,f,g]1\\5s^25p4f^{13}5\,[d,f,g]\,1\\5s5p^24f^{13}5[d,f,g]1\\5s^25p^24f^{12}nl'\\5s^25p4f^{13}nl'\\5s5p^24f^{13}nl'\end{array}\right\} + e^-, \quad (28)$$

$$RT \rightarrow [Pd]\left\{\begin{array}{c}5s^25p^44f^{12}\\5s^25p^34f^{13}\\5s^25p^24f^{14}\\5s5p^44f^{13}\\5s5p^34f^{14}\\5s^25p^34f^{12}5[d,f,g]1\\5s^25p^24f^{13}5\,[d,f,g]\,1\\5s5p^34f^{13}5\,[d,f,g]\,1\\5s^25p^34f^{12}nl'\\5s^25p^24f^{13}nl'\\5s5p^34f^{13}nl'\end{array}\right\} + h\nu. \quad (29)$$

3.3. Total cross section

In order to reproduce the experimental data, it is necessary to know the proportion of each long-lived level. Because these fractions cannot be determined in experiment, we used three different theoretical models to fit the experimental data. The feasibility of these models has been previously verified in W^{5+} calculations.[11]

In the first model (model 1), a statistical weight was assigned to each contributing configuration

$$\sigma^{\rm exp}(E_{\rm e}) = \sum_k c_k \frac{\sum_i \left(2\times {}^kJ_i+1\right)\times {}^k\sigma_i^{\rm th}(E_{\rm e})}{\sum_i\left(2\times {}^kJ_i+1\right)}, \quad (30)$$

where c_k is the fitting coefficients of the metastable states, ${}^kJ_i$ is the total angular momentum for the long-lived levels i of each metastable state k, and ${}^k\sigma_i^{\rm th}(E_{\rm e})$ is the cross section of level i in metastable configuration k.

In the second model (model 2), we assume a Boltzmann distribution of the excitation level population. In this way, Eq. (30) can be modified to

$$\sigma^{\rm exp}(E_{\rm e}) = \sum_k c_k \frac{\sum_{i=1}^m \left(2^kJ_i+1\right)\exp\left[-E_i/(kT)\right]{}^k\sigma_i^{\rm th}(E_{\rm e})}{\sum_{i=1}^m\left(2^kJ_i+1\right)\exp\left[-E_i/(kT)\right]}, \quad (31)$$

where c_k is the fitting coefficients of the metastable states, and E_i is the excitation energy of long-lived levels i. Based on the peak abundance temperature for tungsten ions, the temperature T is 514000 K for W^{9+} ion and 618000 K for W^{10+} ion.[19]

In the third model (model 3), we take each long-lived level into account and assign a scale to each energy level

$$\sigma^{\rm tot}(\varepsilon) = \sum_{i=1}^{r}\lambda_i\sigma_i^{\rm th}(\varepsilon), \quad (32)$$

where r is the number of all energy levels we considered and λ_i are the fitting coefficients which mean proportion of each level i contributing to the total cross section and it has been normalized (i.e., $\sum_{i=1}^r\lambda_i = 1$).

Based on the detailed calculations on the ground and metastable states, we reproduced the total EISI of W^{9+} ion using Eqs. (30)–(32). Ionization signals exist below the ionization threshold 176.6 eV of the W^{9+} ground state, but the ground state does not ionize below its ionization threshold, so the EISI all comes from the metastable states, i.e., the fraction of the ground states below ionization potential should be 0. When above the ionization threshold, considering that the lifetime of the W^{9+} ground state is much longer than the flight time in the experiment, the ground state of W^{9+} has a main fraction. The fractions λ_i by using Eq. (32) are listed in Table 3. A comparison of cross sections obtained in the three models with experimental results[16] is presented in Fig. 15.

Table 3. The fractions λ_i of 37 long-lived levels for W^{9+} ions the model 3.

Level index	Fraction λ_i	
	Energy range (eV)	
	[0, 170]	[170, 5000]
0	0	0.6000
1	0.032	0.0140
2	0.016	0.0020
3	0.024	0.0020
4	0.008	0.0020
5	0	0.0010
6	0	0.0010
7	0	0.0010
8	0	0.0010
9	0	0.0010
10	0.045	0.4100
11	0.045	0.0010
12	0.045	0.0010
13	0.045	0.0010
14	0.045	0.0005
15	0.045	0.0005
16	0.045	0.0005
17	0.045	0.0005
18	0.045	0.0005
19	0.045	0.0005
20	0.045	0.0005
21	0.045	0.0005
22	0.045	0.0005
23	0.045	0.0005
24	0.045	0.0005
25	0.045	0.0005
26	0.045	0.0005
27	0.045	0.0005
28	0.018	0.0005
29	0.018	0.0005
30	0.018	0.0005
31	0.009	0.0005
32	0.009	0.0020
33	0.009	0.0200
34	0.009	0.200
1993	0.018	0.1400
2004	0.002	0.1400

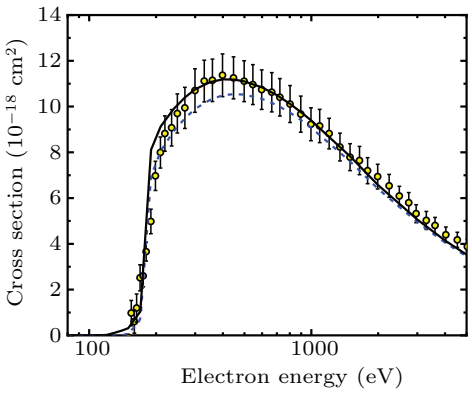


Fig. 15. Comparison of our W^{9+} fitting models with experiments of Stenke *et al.*[18] Yellow circles with error bars: the experimental results of Stenke *et al.*[18] Blue dashed line: the result of model 1. Red dotted line: the result of model 2. Black solid line: the result of model 3.

The theoretical model cross sections resulting from the three models for W^{10+} are represented by the black solid line in Fig. 16. Same as W^{9+}, when the electron energy below the ionization threshold, the fraction of W^{10+} ground states should be 0. And the fractions λ_i by using Eq. (32) are listed in Table 4. The fractions of the other two models for W^{9+} and W^{10+} are listed in Tables 5 and 6, respectively.

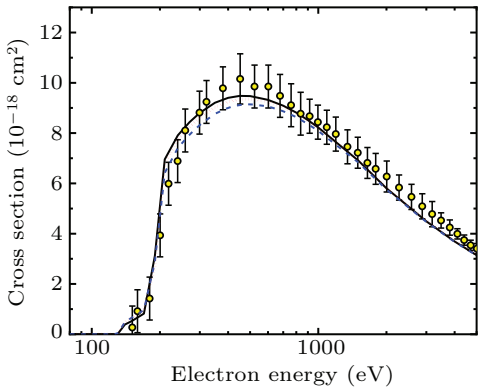


Fig. 16. Comparison of our W^{10+} fitting models with experiments of Stenke *et al.*[18] Yellow circles with error bars: the experimental results of Stenke *et al.*[18] Blue dashed line: the result of model 1. Red dotted line: the result of model 2. Black solid line: the result of model 3.

Table 4. The fractions λ_i of 46 long-lived levels for W^{10+} ions using the model 3.

Level index	Fraction λ_i	
	Energy range (eV)	
	[0, 190]	[190, 5000]
0	0	0.600000
1	0.0080	0.002500
2	0.0800	0.002500
3	0.0080	0.001250
4	0.0640	0.187500
5	0	0.006500
6	0	0.000169
7	0	0.000169
8	0	0.000169
9	0	0.000169
10	0.0208	0.000169
11	0.0208	0.000169
12	0.0208	0.000169
13	0.0208	0.000169
14	0.0208	0.000169
15	0.0208	0.000169
16	0.0208	0.000169
17	0.0208	0.000169
18	0.0208	0.000169
19	0.0208	0.000169
20	0.0208	0.000169
21	0.0208	0.000169
22	0.0208	0.000169
23	0.0208	0.000169
24	0.0208	0.000169
25	0.0208	0.000169
26	0.0208	0.000169
27	0.0208	0.000169
28	0.0208	0.000169
29	0.0208	0.000169
30	0.0208	0.000169
31	0.0208	0.000169
32	0.0208	0.000169
33	0.0208	0.000169
34	0.0208	0.000169
35	0.0208	0.000169
36	0.0208	0.000169
37	0.0800	0.000169
38	0.0208	0.000169
39	0.0208	0.000169
40	0.0208	0.000169
41	0.0208	0.000169
42	0.0208	0.000169
43	0.0208	0.000247
44	0.0336	0.052000
2528	0.0400	0.310000

Table 5. Fractions of W^{9+} ion in model 1 and model 2 (see main text).

Configurations	Model 1		Model 2	
	Energy range (eV)		Energy range (eV)	
	[0, 170]	[170, 5000]	[0, 170]	[170, 5000]
$5p^3$	0.00	0.75	0.00	0.73
$5p^25d$	0.00	0.15	0.00	0.22
$4f^{13}5p^4$	1	0.10	1	0.05

Table 6. Fractions of W^{10+} ion in model 1 and model 2 (see main text).

Configurations	Model 1		Model 2	
	Energy range (eV)		Energy range (eV)	
	[0, 190]	[190, 5000]	[0, 190]	[190, 5000]
$5p^2$	0.00	0.70	0.00	0.70
5p5d	0.05	0.25	0.05	0.28
$4f^{13}5p^3$	0.95	0.05	0.95	0.02

4. Fitting coefficients

We have fitted the calculated total EISI cross sections for convenience in plasma modeling using the following formula:[20]

$$\alpha_{\text{total}}^{\text{EI}_0}(\varepsilon) = \left(\frac{10^{-13}}{\varepsilon I_0}\right)\left(A_0 \ln\left(\frac{\varepsilon}{I_0}\right) + \sum_{i=1}^{8} A_i \left(1-\frac{I_0}{\varepsilon}\right)^i\right), \tag{33}$$

where ε (in eV) is incident electron energy, I_0 (in eV) is the ionization potential and A_i are the fitting coefficients, which are presented in Table 7.

Table 7. Fitting coefficients using Eq. (33) for total EISI cross section. The I_0 used are 131.15 eV and 145.98 eV for W^{9+} and W^{10+} corresponds to the onset of the ionization cross section of the metastable state, respectively.

Coefficients	W^{9+}	W^{10+}
A_0	3.97249	–2.75831
A_1	–5.84552	0.78611
A_2	–13.27231	5.16114
A_3	185.46742	190.33162
A_4	191.62834	–146.47159
A_5	–2868.09075	–1966.8719
A_6	6245.54292	5552.84377
A_7	–5484.4839	–5608.04492
A_8	1760.36396	2012.49647

5. Conclusion and perspectives

We have calculated EISI cross sections of W^{9+} and W^{10+} employing the LLDW method. For the comparison with the experiment results, all long-lived levels both of the ground configuration and metastable configurations are relevant that have lifetimes larger than the flight time of the ions. The previous experiment measurements can be reproduced well particularly when the incident electron energy lower than the ground state ionization potential. The metastable levels could have important influence especially on the edge fusion plasma.

Looking ahead, (i) the contributions of metastable states on the total ionization cross section other low charged W ions or other adjacent elements should be considered in the theoretical calculations and investigations, and (ii) fully treatment of electron correlation to the 4f ground ions is still a very challenge problem. Calculation method with higher accuracy and efficiency is expected as well as the fine energy scan experiment will helpful to improve the understanding of the contribution from metastable states on the total EISI cross section.

Acknowledgements

Project supported by the National Natural Science Foundation of China (Grant No. 11404152) and Fundamental Research Funds for the Central Universities (Grant No. lzujbky-2017-94).

References

[1] Federici G 2006 *Phys. Scr.* **T124** 1
[2] Groth M, Brezinsek S, Belo P, Beurskens M N A, Brix M, Clever M, Coenen J W, Corrigan C, Eich T and Flanagan J 2013 *Nucl. Fusion* **53** 093016
[3] Pitts R A, Carpentier S, Escourbiac F, Hirai T, Komarov V, Lisgo S, Kukushkin A S, Loarte A, Merola M, Sashala Naik A, Mitteau R, Sugihara M, Bazylev B and Stangeby P C 2013 *J. Nucl. Matt.* **438** S48
[4] Putterich T, Neu R, Dux R, Whiteford A D, O'Mullane M and the ASDEX Upgrade Team 2008 *Plasma Phys. Control. Fusion* **50** 085016
[5] Pütterich T, Neu R, Dux R, Whiteford A, O'Mullane M, Summers H and the ASDEX Upgrade Team 2010 *Nucl. Fusion* **50** 025012
[6] Müller A 2015 *Atoms* **3** 120
[7] Pütterich T, Fable E, Dux R, O'Mullane M, Neu R and Siccinio M 2019 *Nucl. Fusion* **55** 056013
[8] Peacock N J, O'Mullane M G, Barnsley R and Tarbutt M 2008 *Can. J. Phys.* **86** 277
[9] kinner C H 2009 *Phys. Scr.* 2009 014022
[10] Zhang D H, Xie L Y, Jiang J, Wu Z W, Dong C Z, Shi Y L and Qu Y Z 2018 *Chin. Phys. B* **27** 053402
[11] Jonauskas V, Kynienė A, Kucas S, Pakalka S, Masys S, Prancikevicius A, Borovik A Jr, Gharaibeh M F, Schippers S and Müller A 2019 *Phys. Rev. A* **100** 062701
[12] Chen L, Li B W and Chen X M 2022 *J. Quant. Spectrosc. Radiat. Transfer* **285** 108179
[13] Yan C L, Lu Q, Xie Y M, Li B L, Fu N, Zou Y, Chen C and Xiao J 2022 *Phys. Rev. A* **105** 032820
[14] Priti, Mita M, Kato D, Murakami I, Sakaue H A and Nakamura N 2020 *Phys. Rev. A* **102** 042818
[15] Lu Q, Yan C L, Fu N, Yang Y, Chen C Y, Xiao J, Wang K and Zou Y 2021 *J. Quant. Spectrosc. Radiat Transfer* **262** 107533
[16] Kramida A, Ralchenko Yu, Reader J and NIST ASD Team (2021). NIST Atomic Spectra Database (ver. 5.8), [Online]. Available: https://physics.nist.gov/asd [2022, May 28]. National Institute of Standards and Technology, Gaithersburg, MD
[17] Gu M F 2008 *Can. J Phys.* **86** 675
[18] Stenke M, Aichele K, Harthiramani D, Hofmann G, Steidl M, Völpel R and Salzborn E 1995 *J. Phys. B* **28** 2711
[19] Preval S P, Badnell N R and O'Mullane M G 2019 *J. Phys. B* **52** 025201
[20] Dipti, Das T, Bartschat K, Bray I, Fursa D V, Zatsarinny O, Ballance C, Chung H K and Ralchenko Yu 2019 *At. Data Nucl. Data Tables* **127–128** 1